Continuous Fabrication of Highly Conductive and Transparent Ag Mesh Electrodes for Flexible Electronics

Zhaozhao Wang, Peiyun Yi, Linfa Peng, Xinmin Lai, and Jun Ni

***Abstract*—Flexible transparent conductive electrodes are essential components for flexible electronics and more functions are combined in such components for miniaturization and design flexibility. The embedded metal mesh, due to the merits of good transparency, conductivity, and flexibility, is regarded as a promising candidate for transparent conductive electrodes. This study reports a continuous fabrication approach of roll-to-roll ultraviolet-nanoimprint lithography (R2R UV-NIL) for the large-area fabrication of embedded Ag mesh electrodes on polyethylene terephthalate (PET) substrates. It has the potential to replace the vacuum-based metal deposition process in flexible transparent electrodes fabrication for large-area, high-throughput, and low-cost production. A R2R UV-NIL system is developed that consists of microchannels patterning stage, doctor blading stage, and Ag residual layer removing stage. A nickel mold for the R2R UV-NIL process is theoretically designed and practically developed. A prototype of embedded metal mesh has been fabricated using water-based, nanosilver paste, and the electrical and optical performance have been further improved by wet etching. The optical transmittance and the sheet resistance are 82.0% and 22.1 Ω/sq, respectively. The electrical and optical performance is excellent with a high $\sigma_{\mathrm{dc}}/\sigma_{\mathrm{opt}}$ value of 81. It is demonstrated that the R2R UV-NIL process is feasible for the large-area fabrication of embedded Ag mesh for flexible transparent electrodes.**

***Index Terms*—Ag mesh electrodes, flexible electronics, roll-to-roll, UV-nanoimprint lithography.**

I. Introduction

FLEXIBLE electronics have been regarded as the next generation in optoelectronic devices in various areas, such as 3D molded interconnect (MID) devices, flexible displays, wearable electronics, organic light-emitting diodes (OLED), organic solar cells and radio-frequency identification chips and circuits. The new generation of optoelectronic devices can be bent, compressed and deformed into various shapes while maintaining good performance and this concept has been originally proposed by L. J. Guo and other scholars at the University of Michigan as a pioneer of this field [1]. Transparent electrodes are essential components for optoelectronic devices and the deposition of indium tin oxide (ITO) on various substrates is the conventional approach. Although ITO has exhibited desirable optical and electrical performance, the film brittleness and low abundance of ITO are still the main concern of optoelectronic industry. The rigidity of ITO-coated glass has severely restricted their suitability for use in flexible optoelectronic devices. Besides, the increasing cost of indium hinders the high-throughput production of ITO transparent electrodes [2].

In recent years, conducting polymers [3], graphene films [4]–[6], carbon nanotube networks [7]–[9], conductive nanowire [10]–[13] and metal mesh have been widely studied as alternative materials for transparent flexible electrodes in both industry and academia. Among them, patterned silver mesh is a promising candidate due to its good transparency, conductivity and flexibility. Embedding Ag mesh into a transparent substrate has the following remarkable advantages: (1) the cross-section morphology and the height-to-width ratio of Ag mesh lines can be controlled; (2) the topology of the mesh pattern built on the transparent substrate can also be controlled. Both aspects are beneficial to enhance the accuracy of sensors when applied to flexible touch panel sensors. Currently, thermal R2R imprint lithography, roll offset printing process and transfer printing process are existing technologies to fabricate the transparent metal mesh electrodes. Scholars have made great efforts to demonstrate the effectiveness of these technologies in fabricating transparent mesh electrodes in batch mode. Yao *et al.* [14] developed a rubber-assisted hot embossing process for uniform shell patterning. S. Kim *et al.* [15] systematically discussed the main factors that affect embossed pattern qualities of R2R hot embossing. Yu *et al.* [16] first introduced thermal R2R lithography to manufacture transparent conductive film. Deng *et al.* [17]–[19] fabricated complex functional micro-structures on PVC substrates using thermal R2R lithography. Kim *et al.* [20] presented a low cost, high-throughput procedure for the

Manuscript received March 9, 2017; revised May 7, 2017; accepted May 13, 2017. Date of publication May 17, 2017; date of current version July 7, 2017. This work was supported by the National Natural Science Foundation of China under Grants 51235008, 51675334, and 51522506. The review of this paper was arranged by Associate Editor J. T. W. Yeow. *(Corresponding authors: Peiyun Yi; Jun Ni.)*

Z. Wang, P. Yi, and L. Peng are with the State Key Laboratory of Mechanical System and Vibration, Department of Mechanical Engineering, Shanghai Jiao Tong University, Shanghai 200240, China (e-mail: wangzhaozhao@sjtu.edu.cn; yipeiyun@sjtu.edu.cn; penglinfa@sjtu.edu.cn).

X. Lai is with the State Key Laboratory of Mechanical System and Vibration, Department of Mechanical Engineering and State Key Laboratory of Digital Manufacture for Thin-walled Structures, Shanghai Jiao Tong University, Shanghai 200240, China (e-mail: xmlai@sjtu.edu.cn).

J. Ni is with the Shien-Ming Wu Manufacturing Research Center, Department of Mechanical Engineering, University of Michigan, Ann Arbor, MI 48109 USA (e-mail: juni@umich.edu).

Color versions of one or more of the figures in this paper are available online at http://ieeexplore.ieee.org.

Digital Object Identifier 10.1109/TNANO.2017.2705173

fabrication of transparent and flexible silver electrodes on a submicron scale. Kim *et al.* [21] demonstrated that roll-offset printing process can be used to manufacture transparent conducting electrodes for organic solar cells. Lee *et al.* [22] demonstrated a high-durable AgNi nanomesh that exhibited strong adhesion by using simple transfer printing. Jang *et al.* [23] fabricated a metal (Ag) grid/AgNW hybrid TCE film composed of an electroplated metal grid and surface embedded AgNW networks with excellent opto-electrical performance (transparency of 87% and sheet resistance of 13 Ω/sq). Khan *et al.* [24] proposed a new type of electroplated copper nanomesh with superior electrical conductivity and optical transmittance. Kwon *et al.* [25] used monolayers of PS spheres with different diameters as the template to create Ag honeycomb mesh electrodes. Hong *et al.* [26] introduced a nonvacuum, maskless fabrication technique of a flexible metal grid transparent conductor by low-temperature selective laser sintering of nanoparticle ink. Han *et al.* [27] invented a uniform self-forming metallic network as a high performance transparent conductive electrode. However, it is still a big challenge to produce the large-area metal mesh with line widths of submicron or even nano scale with continuous mode in non-vacuum environment.

In this study, a continuous fabrication approach of roll-to-roll ultraviolet-nanoimprint lithography (R2R UV-NIL) is proposed for the large-area production of metal mesh patterns for flexible transparent electrodes. A R2R UV-NIL nanoimprinting system is first introduced and the mold is well developed. High quality metal mesh samples are fabricated for demonstration by doctor blading nano-silver paste into narrow channels. The morphology of the Ag mesh at different fabrication stages are characterized. Besides, the influence of UV-NIL process parameters on optical transmission performance is investigated and discussed. Thereafter, the electrical and optical performance have been evaluated and both performance are further improved by manipulating process conditions such as wet etching. Finally, the mechanical and environmental stabilities of the Ag mesh are further assessed. The objective of this study is to exhibit the feasibility of R2R UV-NIL for fabrication of flexible and transparent Ag mesh electrodes and to propose a new type of embedded metal mesh with high performance, good mechanical and environmental stabilities for flexible electronics.

II. Experimental Section

A. R2R UV-NIL Setup

As shown in Fig. 1(a), the fabrication process of metal mesh arrays using R2R UV-NIL for flexible transparent electrodes mainly consists of three processes: (1) continuous R2R UV-NIL process to pattern channels of small widths (less than 10 μm) on UV-curable resin; (2) the doctor blading methodology could be used to fill the conductive Ag paste into the narrow channels; (3) the Ag residual layer could be removed from the surface of the cured resin so that the transparency of the electrode could be improved. The R2R UV-NIL process mainly consists of the filling stage, the UV illumination stage and the demolding stage. The UV resin coating process is a tape casting process. A doctor is located parallel above the PET substrate and a gap is kept between the doctor and the PET substrate to confirm the uniformity of the UV resin covered on the substrate. Under the web tension and the pressure from the backup roller, the UV resin with low viscosity quickly fills into mold cavity at the filling stage. Then the resin-coated PET substrate wrapped on the mold roller is exposed to UV illumination. Finally, the PET substrate with roller-imprinted microstructures is continuously separated from the mold roller via the release roller at the demolding stage.

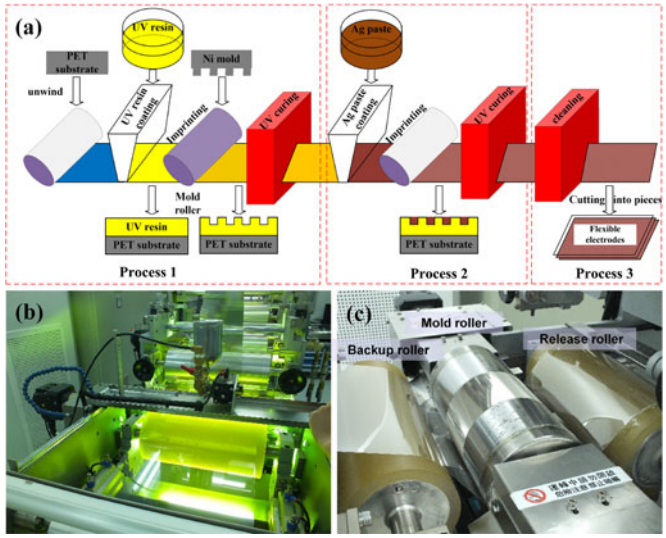

Fig. 1. (a) The schematic of manufacturing process for the flexible electrodes by R2R UV-NIL. (b) The R2R UV-NIL system. (c) The forming unit.

TABLE I
Specifications of the Self-Developed R2R UV-NIL System

Specifications	Value
Size of the rubber roller (mm)	Φ160 × 350
Size of the forming roller (mm)	Φ160 × 350
Feeding speed (m min^{-1})	0–20
Pressure of the rubber roller (kg cm^{-2})	0.05–6
Tension force of the PET substrate (kg)	0–50
Central temperature of the forming roller (°C)	0–120
Power of UV lamp (W)	7000

As shown in Fig. 1(b) and (c), a R2R UV-NIL system has been designed and developed in our lab. The dispensing unit has the function of coating the UV-curable resin onto the transparent substrate. The UV power unit illuminates the curing region where the roller-attached mold and UV resin on the substrate make contact and the cavity of the roller mold is filled with UV resin. The rotational velocities of the mold roller and the other rollers are controlled with a stepping motor and a gear system. Also the mold roller has the function of heating the UV resin. The specifications of the R2R UV-NIL system are listed in Table I.

B. Materials & Mold

The PET substrate has high transparency, good mechanical flexibility and low cost so that they are widely used in industrial production. In this study, the PET thickness is 100 μm and the

TABLE II
THE SUMMARY OF MATERIALS AT ROOM TEMPERATURE (25 °C)

Materials	Transmittance	Dimension	Refraction	Concentration	Viscosity(cps)
PET	91%	100 μm	1.54	–	–
UV-curable Resin(PHQ53A)			1.545	–	322.3
Ag Paste	–	–	–	85wt.%	3500

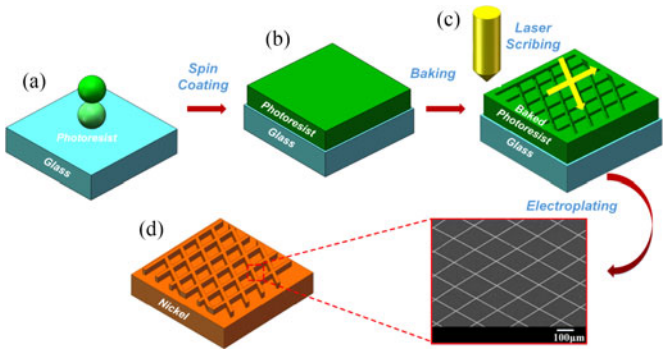

Fig. 2. Schematic illustration of the Nickle mold: (a) The photoresist layer on the glass substrate was obtained from spin coating process. (b) The photoresist layer was baked. (c) Trenches on resin layer were obtained by laser scribing process. (d) The nickel mold was obtained from electroplating process. Inset: SEM image of the nickel mold.

average transmittance is 91.3%. The Ag paste has an average diameter of 100 nm and the silver contents weight is 85%. The UV-curable resin (PHQ53A) and PET films used in our experiments have been provided by Jiangsu Kangde Xin Composite Material Co., Ltd. The Ag (85 wt%) paste has been purchased from NANO TOP Co., Ltd. Besides, inks with particles of a few micrometers in size could not fill the narrow channels compactly, so inks with nano-sized particles are required. Physical properties of the Ag paste, viscosity and yield strength are controlled to make the doctor blading process feasible. The UV-curable resin used in the R2R UV-NIL process can quickly change from liquid state to solid state by the activation of UV illumination. Table II shows the summary of materials at room temperature (25 °C) [28].

In this study, a 500 × 250 mm^2 Ni mold with an array of 90 × 55 mm^2 via photolithography process has been developed aiming at 4 flexible touch screens in axial direction. Scholars have made great efforts to develop effective micromolding processes. He *et al.* have developed Si micro-mold via photolithography process for the fabrication of CNT-carbon composite microstructures [29]. Zhou *et al.* have fabricated carbon/CNT composite microcantilevers using Si micro-mold fabricated via photolithography process [30]. An *et al*. have developed novel electroplating methods for the synthesis of CNTs/Ni nanocomposite [31]. Fig. 2 presents the fabrication process of the nickel mold. In a typical fabrication process of the Ni mold, firstly a photoresist AZ4562 layer with the thickness of approximately 10 μm was spin coated on the glass substrate with the speed of 1700 r/min for 30 s (Laurell spin coater, America). Then the photoresist AZ4562 layer was baked with the temperature of 95 °C for 25 min [32]. In the following step the baked photoresist was exposed in the Heidelberg DWL 66+ laser direct-writing system and narrow channels with width of micros were obtained on the baked photoresist via laser scribing process. In the following electroplating step, a thin Ag layer was deposited on the baked photoresist pattern to make it conductive through the physical vapor deposition, then nickel metal was deposited inside onto the resist template and filled the trenches with a uniform mesh structure in the nickel plating solution. The nickel plating solution was composed of 0.9 kmol/m^3 $NiSO_4$, 0.99 kmol/m^3 $NiCl_2$ and 0.5 kmol/m^3 H_3BO_3. The PH value of the nickel plating solution was set as 2.8. The plating current density was 100 A/m^2 and the plating time lasted one minute. In the following step, the photoresist was dissolved in the KOH/ethanol solvent after 15 minutes, leaving a nickel mesh template. The KOH/ethanol was obtained by dissolving 16 g KOH in 30 ml water and adding 20 ml ethanol into the solution. The mold plate which has straight raised ridges with rectangular-shaped cross section on its surface was made of Nickel metal. The heights and the widths of the rectangular-shaped ridges basically determine the depths and widths of the micro-channels on the cured resin. Besides, the surface roughness of the mold plate has great influence on the uniformity of the surface of the micro-channels.

The optical transmittance of the printed mesh arrays including the substrate can be calculated using the design parameters of the grid spacing a and the linewidth d. The optical transmittance of Ag grid mesh can be expressed as follows:

$$T = T_{sub} \times (1 - f)^2 \tag{1}$$

where $f = d/a$. Similarly, the sheet resistance of the transparent electrodes is also determined by the design factors, Ag mesh height h, grid spacing a, linewidth d and the conductivity σ. Then the sheet resistance can be deduced as:

$$R_s = 1/(fh\sigma) \tag{2}$$

The figure of merit (FOM) introduced here is [33]:

$$\phi = T^{10}/R_s \tag{3}$$

The figure of merit (FOM) can also be written as follows:

$$\phi = {T_{sub}}^{10} \times (1 - f)^{20} \times f \times h \times \sigma \tag{4}$$

where A is a constant, ϕ can be approximated by using Newton's binomial theorem [33].

$$\phi \approx A \times (f - 20f^2) \tag{5}$$

ϕ is maximized by calculating as follows:

$$d\phi/df = A \times (1 - 40f) = 0 \tag{6}$$

Then f value is obtained:

$$f = 1/40 \tag{7}$$

For the highest FOM, the ratio of grid spacing to linewidth is approximately 40. In this study the mold is fabricated based on the proposed design criteria. The proposed design is experimentally evaluated in the following session.

C. Preparation of Ag Mesh Electrodes

The substrates with micro-channels on it were prepared via the R2R UV-NIL process firstly. Ag paste was doctor bladed into the narrow channels on the substrate, and then it was preheated on a hot plate at 140 °C for 2 min. The Ag paste was again doctor bladed into the narrow channels to fully fill it. The curing temperature was 140 °C and it lasted 30 min. Before Ag paste filling stage, plasma treatment had improved the hydrophilic property of the UV-resin covered substrate. The sidewalls of these micro-channels structures were hydrophobic [34]. Thus, the plasma treatment before Ag paste doctor blading process was necessary. The low pressure plasma treatment lasted 2 minutes was performed using Diener Plasma Instrument FEMTO. In the following stage, the residual Ag layer was wet etched by immersing the Ag mesh in nitric acid (15%) to reduce the residues on the Ag mesh surface. After wet etching, the Ag mesh was immersed in DI water and blown under nitrogen. The transmittance and sheet resistance of the Ag mesh were recorded as a function of immersing time in nitric acid (15%).

D. Optical, Electrical and Microscopic Characterization

Optical transmittance was measured using a UV-vis spectrophotometer(EV300). The sheet resistance of the Ag mesh electrodes was investigated by a four-point probe system(Hiresta-UX, MCP-T370). SEM images were taken using JEOL JSM-7800F Prime(SEM) & Thermo ScientificTM NORANTM Syst. The topology and cross-sectional scans were measured using an atomic force microscope (NT-MDT NETGRA, AFM).The dimensions of the mold and inset in Fig. 5 were measured and taken via KEYENCE 3D Laser Scanning Confocal Microscope.

E. Bending, Adhesion & Environmental Stability Test

For the bending test, firstly the Ag mesh electrodes were fixed on a cylinder of different curvature radius (5 mm, 10 mm) with the inner face of the Ag mesh (compressively) or the back face of the Ag mesh (tensile) facing the convex side of the cylinder. Then all Ag mesh electrodes were repeatedly bent by an automatic bending device. The sheet resistance of all bending samples was recorded.

For the adhesion test, an adhesive polypropylene tape with acrylic adhesive was pressed onto the surface of the Ag mesh electrodes and slowly peeled off. The process was repeated several times to confirm the adhesion property of the Ag mesh electrodes. Then the sheet resistance of these samples was measured after every 20 peeling tests.

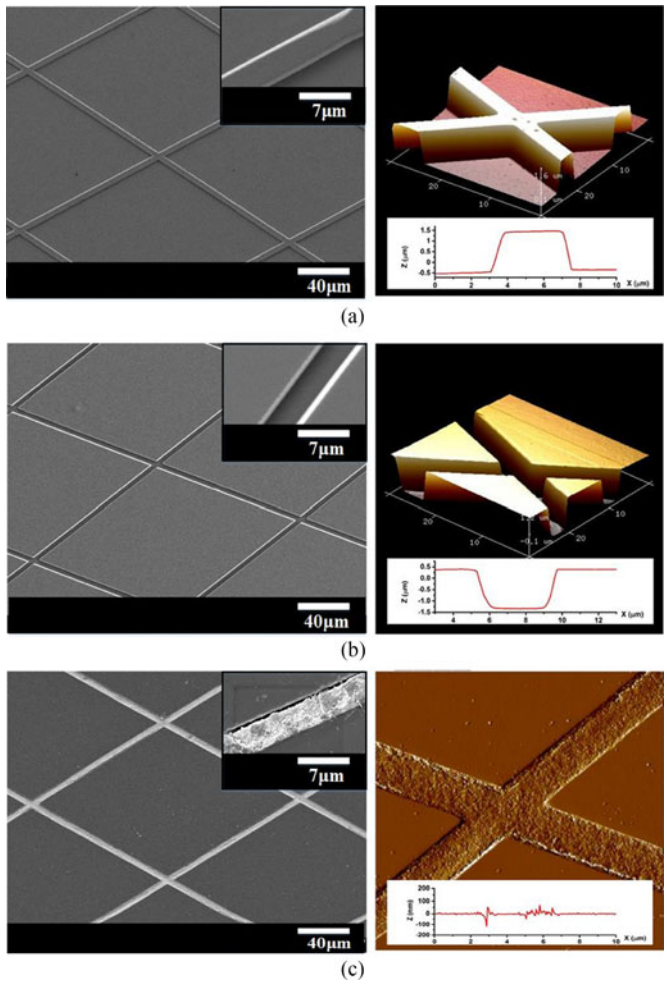

Fig. 3. Morphological characterization by SEM(left) and AFM(right) of an Ag mesh electrode at different fabrication stages: (a) Nickel mold. (b) NIL imprinted micro channels on the PET substrate. (c) Ag mesh embedded on the PET substrate.

To prepare the environmental stability test, these tested Ag mesh electrodes were immersed into deionized (DI) water or were exposed to high-temperature and high-humidity conditions (65 °C, 75% relative humidity) for 24 hours. Then the sheet resistance of these samples was recorded every 2 hours.

III. Results and Discussions

A. Morphological Characterization

Fig. 3 shows the AFM 3D plot and cross-sectional scans of an imprinted channel and the channel would be filled with nano-silver pastes after doctor blade process. As shown in Fig. 3(a), there are straight-ridges features with rectangular cross sections on the flexible Ni mold. As shown in Fig. 3(b), the imprinted channel has a depth of 1.6 μm and a width of 3.5 μm. As shown in Fig. 3(c), the top surface of the metal mesh is on the same level as the substrate surface and the surface roughness for the Ag mesh measured is approximately 150 nm, which results in an expected uniform film thickness in touch sensors. This is the reason that embedded metal mesh is used for the fabrication of

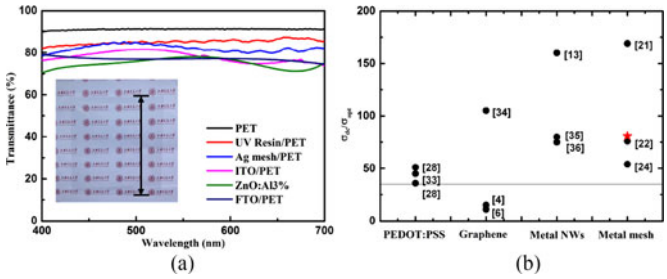

Fig. 4. (a) UV-vis spectra of Ag mesh electrode on PET film, the UV resin-covered PET film, the Ag mesh covered PET film, the ITO covered PET and the FTO covered PET and the Al (3%) doped ZnO film, with optical image shown in the set. (b) Comparison of the FOM (σ_{dc}/σ_{opt}) values for transparent electrodes of PEDOT:PSS, graphene, metal nanowires, and metal mesh. The stars indicate the experimental results obtained in this study.

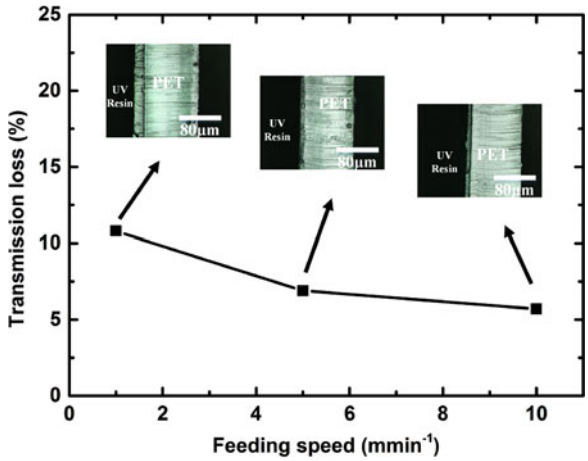

Fig. 5. Transmission loss of Ag mesh electrodes in UV-NIL process with imprinting pressure of 3 kg cm^{-2} and mold temperature of 25 °C. Inset: Cross section image of UV resin-coated PET substrate.

transparent electrodes, though excess step of channel fabrication is required in addition to the Ag paste printing process. AFM measurements have revealed a depth of 300 nm in the channels resulting from the shrinkage and evaporation of the Ag paste solvent. The concave shape with a deepness of about 300 nm is caused by the coffee ring effect during the heat treatment process. It appears that there are some parasitic Ag islands along the narrow channels which is inevitable and has no negative effects on the applications of the transparent electrodes, as the heights of such Ag islands are within the range of 50 nm.

B. Electrical and Optical Characterization of Ag Mesh Electrodes

The proposed fabrication process can be applied to metal meshes with micrometer feature sizes, which benefit many optoelectronic applications by providing improved visibility and conductivity. Flexible transparent electrodes with good conductivity can meet the low power density and rapid response time requirements of many optoelectronic applications. The transparency of the flexible transparent electrodes also contributes to the performance of many optoelectronic applications. Thus, it is necessary to evaluate the electrical and optical performance quantitatively. Traditionally, evaluating methods of the optical transmittance and sheet resistance performances consist of the evaluation criteria of the electrical and optical performances of flexible transparent electrodes.

1) Electrical and Optical Performance: The optical transmittance of the embedded Ag mesh electrode on resin-covered PET substrates within the visible wavelength range was measured and shown in Fig. 4(a), and the optical transmittance spectra of the resin-covered PET substrates and the bare PET films were shown as references. The optical transmittance spectra of the fluorine tin oxide (FTO)-covered PET substrates with the sheet resistance of 15 Ω/sq and Al (3%) doped ZnO films were also illustrated [15]. All the transmittance measurements have been conducted in air. The average transmittance of the Ag mesh electrode is about 82.0%, higher than that of the FTO-covered PET substrates and Al (3%) doped ZnO films. The optical performance has also been compared with those of ITO-deposited PET film with ITO thickness of 160 nm [15]. The PET/ITO has shown a relative large transmission loss in the visible wavelength region. The transmittance of PET/Ag-mesh film only decreases 3.1% compared with that of the resin-covered PET substrate.

To gain a direct measurement of optical and electrical performance for the transparent conductor, the figure of merit (FOM), defined as the ratio of the electrical conductance and the optical conductance (σ_{dc}/σ_{opt}), is introduced.

$$T = \left(1 + \left(188.5/R_s\right)\left(\sigma_{dc}/\sigma_{opt}\right)\right)^{-2} \tag{8}$$

where R_s and T are the measured sheet resistance and transmittance at 550 nm, respectively [19]. The FOM of actual metal mesh calculated with the measured sheet resistance and averaged transmission is 81. The FOM of ITO is about 44. Thus, the Ag mesh has a better optical and electrical performance than ITO film. The black horizontal line with a FOM value of 35 indicates the minimum value for most transparent conductive electrodes (TCEs) applications. Fig. 4(b) also shows the FOM values of poly-(3,4-ethylenedioxythiophene): poly(styrenesulfonate)(PEDOT:PSS) [35], [36], graphene [4], [6], [37], metal nanowires [13], [38], [39] and various metal meshes [19], [20], [22]. The FOM value obtained in our study is as good as that of metal nanowires and it is higher than the minimum FOM value of most TCE applications.

2) Effect of UV-NIL Feeding Speed: The precision of the UV resin-coated substrates basically determines the performance of Ag mesh electrodes and the tuning of process parameters has big influence on the performance of Ag mesh electrodes. Thus, during the UV-NIL process, the imprinting pressure, temperature and feeding speed should be controlled depending on the type of resin materials and pattern shapes. Both the control of process parameters and the physical properties of Ag paste contribute to a highly conductive transparent film. The patterning quality of the patterned substrates is mainly determined by the feeding speed [40]. Three UV-NIL tests have been conducted with three different feeding speeds. The other parameters relating the UV-NIL process and doctor blading process have remained constant. The printability of the substrates has been

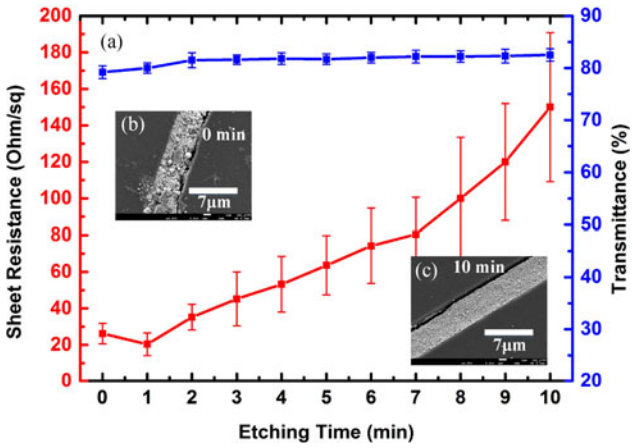

Fig. 6. (a) Variations in sheet resistance and transmittance versus the etching time, Inset (b) and (c): SEM images before etching and after 10 min's etching.

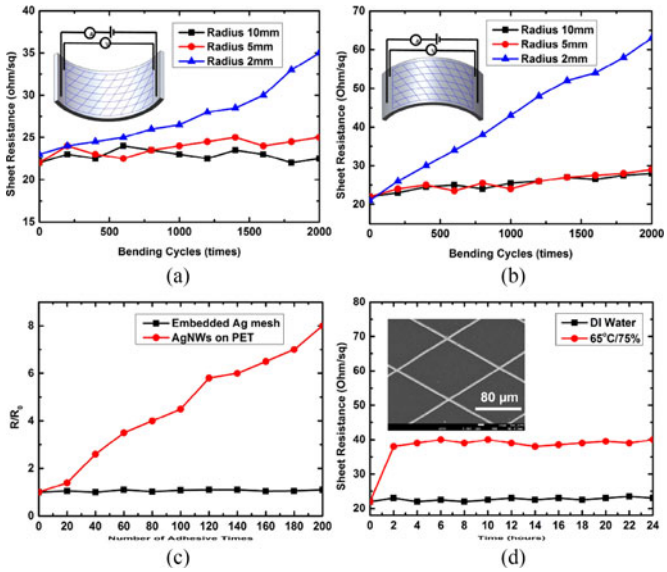

Fig. 7. Mechanical stability of the Ag mesh electrodes. (a) Variations in sheet resistance versus the number of cycles of repeated compressive bending to radii of 10, 5, and 2 mm. (b) Variations in sheet resistance versus the number of cycles of repeated tensile bending to radii of 10, 5, and 2 mm. (c) Variations in sheet resistance during the repeated adhesive tape test. (d) Variations in sheet resistance during the chemical and environmental stability tests. Inset: SEM images after the tests.

quantitatively evaluated by measuring the optical transmittance of the printed patterns. Fig. 5 shows the transmission loss measured from each printing sample. The transmission loss refers to the transmission reduction percentage of each sample compared with the PET substrate at wavelength of 550 nm. Transmission loss decreases as feeding speed increases. The highest operating speed yields minimum transmission loss. The transmission loss mainly arises from the blocking of the UV-resin layer. Under high feeding speed the UV-curable resin rapidly spreads on PET substrates, resulting in thinner UV-resin layer. Inset shown in Fig. 5 demonstrates that thinner UV-resin layer corresponds to lower transmission loss.

3) Effect of Ag Etching Time: The electrical and optical performance could be improved by wet etching Ag mesh in nitric acid. Since the parasitic Ag islands degrade the transmittance, wet etching technique could be used to control the area covered by parasitic Ag islands [25]. Fig. 6(a) shows the variation of transmittance and the average sheet resistance as Ag etching time proceeds. Wet etching for 2 min increases the sheet resistance from 26.2 to 35.2 Ω/sq by decreasing the Ag mesh thickness. The sheet resistance decreases abruptly in the earlier etching time and increases later. The reduction of the sheet resistance from 26.2 to 35.2 Ω/sq at the beginning of the wet etching process is due to eliminating oxidized residues and by-products. Whereas the transmittance slightly increases from 79.2% to 81.5% at the same time. The increase in transmittance is due to fewer Ag islands. The decrease of the sheet resistance in the early etching time is also due to fewer Ag islands. The increase in sheet resistance is depended on decrease in Ag mesh thickness. The remaining parasitic Ag islands have been minimized by wet etching. As shown in Fig. 6(b) and (c), parasitic Ag islands have been mostly eliminated by a 10 min wet etching pretreatment. The conductivity improves 10 percentage points while the transmittance improves only 2 percentage points when these properties are improved by optimization in wet etching process.

C. Mechanical and Environmental Stability

In addition to good electrical and optical performance, the embedded metal mesh electrodes also have strong adhesion to substrates due to large-area contacts with the substrates and good mechanical stabilities under tensile and compressive loading. Fig. 7(a) shows variations in sheet resistance as a function of the number of cycles of repeated compressive bending with radii of 10, 5 and 2 mm. For the compressive bending radii of 10 and 5 mm, there is no noticeable change in sheet resistance within cyclic loading of 2000 cycles. For the compressive bending radii of 2 mm, the value of sheet resistance increases 50 percent. Similarly, as shown in Fig. 7(b), for the tensile bending radii of 10 and 5 mm, the sheet resistance just varies by 30 percent within cyclic loading of 2000 cycles. For the tensile bending radii of 2 mm, the value of sheet resistance increases 200 percent. The high increase in sheet resistance is due to crack of the Ag mesh structure under high tensile stress. It can be concluded that the embedded type metal mesh is easier to be broken under tensile stress than under compressive stress.

The mechanical stabilities of the Ag mesh electrodes have been also demonstrated by a repeated adhesive tape test. The repeatedly adhesive tape test has been performed to evaluate the adhesion between the Ag mesh and the substrate. As shown in Fig. 7(c), the sheet resistance of the embedded Ag mesh remains to be unchanged after 200 cycles, whereas the sheet resistance of AgNW increases significantly. The reason that Ag mesh is strongly adhesive to the substrate is that Ag is partially embedded into the UV resin. To evaluate the long-term stability of the Ag metal mesh, the environmental stability of the Ag mesh has been conducted by immersing them into deionized (DI) water and exposing them to high-temperature and high-humidity conditions (65 °C, 75% relative humidity). Fig. 7(d) shows the variations of sheet resistance of the Ag mesh every 2 hours. At the beginning of the environmental test, the increase of the sheet

resistance is due to the non-isothermal operation via changing the Ag mesh electrodes' environmental temperature from room temperature (25 °C) to higher temperature (65 °C). After 24h, the morphological structures and the sheet resistance remain unchanged under such testing conditions. Both the mechanical stability and the environmental stability confirmed in these tests have been attributed to the embedded nature of the Ag mesh electrodes, for which the Ag mesh electrodes are confined to narrow channels and three faces of the Ag mesh have been isolated from air.

IV. Conclusion

In summary, flexible transparent electrodes with embedded Ag mesh were fabricated by R2R UV-NIL process. Microchannels with the average width of 3.5 μm formed on the PET substrates were coated with cured UV resin. The solvent-based Ag paste composed of nano-size silver particles was used to fill the channels via a doctor blading process and Ag paste in the channels was cured with heat treatment. Finally, the Ag residue on the PET substrate was removed by use of dilute nitric acid. The influences of the R2R UV-NIL process parameters, including the influence of the feeding speed on the optical transmittance of Ag mesh electrodes, are the discussion point in this study, which has great importance on the industrial production of Ag mesh flexible electrodes. The optical and electrical performance of the Ag mesh electrodes are 82.0% in transmittance and 22.1 Ω/sq in sheet resistance and these performances could be further improved by optimization of the mesh structures and fabrication strategy. These transparent electrodes fabricated using such R2R solution process seem to be a promising alternative for flexible electronics. The limitation of this work is that extra step of eliminating the residual Ag layer is required. For future work, the limitation will be overcome by using transparent conductive resin instead of Ag paste. And this process will be employed for the fabrication of flexible electrodes with antireflection structures to get desirable optical transmittance.

References

[1] M. G. Kang, H. J. Park, S. H. Ahn, T. Xu, and L. J. Guo, "Toward low-cost, high-efficiency, and scalable organic solar cells with transparent metal electrode and improved domain morphology," *IEEE J. Sel. Topics Quantum Electron.*, vol. 16, no. 6, pp. 1807–1820, Nov./Dec. 2010.

[2] L. G. De Arco, Y. Zhang, C. W. Schlenker, K. Ryu, M. E. Thompson, and C. Zhou, "Continuous, highly flexible, and transparent graphene films by chemical vapor deposition for organic photovoltaics," *ACS Nano*, vol. 4, no. 5, pp. 2865–2873, 2010.

[3] H. Wu *et al.*, "A transparent electrode based on a metal nanotrough network," *Nat. Nanotechnol.*, vol. 8, no. 6, pp. 421–425, 2013.

[4] S. Bae *et al.*, "Roll-to-roll production of 30-inch graphene films for transparent electrodes," *Nat. Nanotechnol.*, vol. 5, no. 8, pp. 574–578, 2010.

[5] J. Wang, M. Liang, Y. Fang, T. Qiu, J. Zhang, and L. Zhi, "Rod-coating: towards large-area fabrication of uniform reduced graphene oxide films for flexible touch screens," *Adv. Mater.*, vol. 24, no. 21, pp. 2874–2878, 2012.

[6] X. Li *et al.*, "Large-area synthesis of high-quality and uniform graphene films on copper foils," *Science*, vol. 324, no. 5932, pp. 1312–1314, 2009.

[7] R. C. Tenent *et al.*, "Ultrasmooth, large-area, high-uniformity, conductive transparent single-walled-carbon-nanotube films for photovoltaics produced by ultrasonic spraying," *Adv. Mater.*, vol. 21, no. 31, pp. 3210–3216, 2009.

[8] Z. Wu *et al.*, "Transparent, conductive carbon nanotube films," *Science*, vol. 305, no. 5688, pp. 1273–1276, 2004.

[9] Y. Liu *et al.*, "Enhanced photoelectrochemical properties of Cu_2O-loaded short TiO_2 nanotube array electrode prepared by sonoelectrochemical deposition," *Nano-Micro Lett.*, vol. 2, no. 4, pp. 277–284, 2010.

[10] J. van de Groep, P. Spinelli, and A. Polman, "Transparent conducting silver nanowire networks," *Nano Lett.*, vol. 12, no. 6, pp. 3138–3144, 2012.

[11] L. Hu, H. S. Kim, J.-Y. Lee, P. Peumans, and Y. Cui, "Scalable coating and properties of transparent, flexible, silver nanowire electrodes," *ACS Nano.*, vol. 4, no. 5, pp. 2955–2963, 2010.

[12] S. Kiruthika, R. Gupta, K. D. M. Rao, S. Chakraborty, N. Padmavathy, and G. U. Kulkarni, "Large area solution processed transparent conducting electrode based on highly interconnected Cu wire network," *J. Mater. Chem. C*, vol. 2, no. 11, pp. 2089–2094, 2014.

[13] P. Lee *et al.*, "Highly stretchable and highly conductive metal electrode by very long metal nanowire percolation network," *Adv. Mater.*, vol. 24, no. 25, pp. 3326–3332, 2012.

[14] P. Nagarajan and D. Yao, "Uniform shell patterning using rubber-assisted hot embossing process. I. Experimental," *Polym. Eng. Sci.*, vol. 51, no. 3, pp. 592–600, 2011.

[15] S. Kim, Y. Son, H. Park, B. Kim, and D. Yun, "Effects of preheating and cooling durations on roll-to-roll hot embossing," *Microsc. Microanal.*, vol. 21, no. 1, pp. 164–171, 2014.

[16] J.-S. Yu *et al.*, "Transparent conductive film with printable embedded patterns for organic solar cells," *Sol. Energy Mater. Sol. Cells*, vol. 109, pp. 142–147, 2013.

[17] Y. Deng, P. Yi, L. Peng, X. Lai, and Z. Lin, "Experimental investigation on the large-area fabrication of micro-pyramid arrays by roll-to-roll hot embossing on PVC film," *J. Micromech. Microeng.*, vol. 24, no. 4, 2014, Art. no. 045023.

[18] Y. Deng, P. Yi, L. Peng, X. Lai, and Z. Lin, "Flow behavior of polymers during the roll-to-roll hot embossing process," *J. Micromech. Microeng.*, vol. 25, no. 6, 2015, Art. no. 065004.

[19] J. Wang, P. Yi, Y. Deng, L. Peng, X. Lai, and J. Ni, "Recovery behavior of thermoplastic polymers in micro hot embossing process," *J. Mater. Process. Technol.*, vol. 243, pp. 205–216, 2017.

[20] G. Kim, J.-H. Shin, H.-J. Choi, and H. Lee, "Fabrication of transparent and flexible Ag three-dimensional mesh electrode by thermal roll-to-roll imprint lithography," *J. Nanoparticle Res.*, vol. 16, no. 9, pp. 1–6, 2014.

[21] I. Kim *et al.*, "Roll-offset printed transparent conducting electrode for organic solar cells," *Thin Solid Films*, vol. 580, pp. 21–28, 2015.

[22] H.-J. Kim *et al.*, "High-durable AgNi nanomesh film for a transparent conducting electrode," *Small*, vol. 10, no. 18, pp. 3767–3774, 2014.

[23] J. Jang, H.-G. Im, J. Jin, J. Lee, J.-Y. Lee, and B.-S. Bae, "A flexible and robust transparent conducting electrode platform using an electroplated silver grid/surface-embedded silver nanowire hybrid structure," *ACS Appl. Mater. Interfaces*, vol. 8, no. 40, pp. 27035–27043, 2016.

[24] A. Khan *et al.*, "High-performance flexible transparent electrode with an embedded metal mesh fabricated by cost-effective solution process," *Small*, vol. 12, no. 22, pp. 3021–3030, 2016.

[25] K. Namyong, K. Kyohyeok, S. Sihyun, Y. Insook, and C. Ilsub, "Highly conductive and transparent Ag honeycomb mesh fabricated using a monolayer of polystyrene spheres," *Nanotechnology*, vol. 24, no. 23, 2013, Art. no. 235205.

[26] S. Hong *et al.*, "Nonvacuum, maskless fabrication of a flexible metal grid transparent conductor by low-temperature selective laser sintering of nanoparticle ink," *ACS Nano*, vol. 7, no. 6, pp. 5024–5031, 2013.

[27] B. Han *et al.*, "Uniform self-forming metallic network as a high-performance transparent conductive electrode," *Adv. Mater.*, vol. 26, no. 6, pp. 873–877, 2014.

[28] H. Wu, P. Yi, L. Peng, and X. Lai, "Study on bubble defects in roll-to-roll UV imprinting process for micropyramid arrays. I. Experiments," *J. Vacuum Sci. Technol. B.*, vol. 34, no. 2, 2016, Art. no. 021201.

[29] L. He *et al.*, "Fabrication of CNT-carbon composite microstructures using Si micromolding and pyrolysis," *Microsyst. Technol.*, vol. 20, no. 2, pp. 201–208, 2014.

[30] Z. An, L. He, M. Toda, G. Yamamoto, T. Hashida, and T. Ono, "Microstructuring of carbon nanotubes-nickel nanocomposite," *Nanotechnology*, vol. 26, no. 19, 2015, Art. no. 195601.

[31] P. Zhou *et al.*, "The Young's modulus of high-aspect-ratio carbon/carbon nanotube composite microcantilevers by experimental and modeling validation," *Appl. Phys. Lett.*, vol. 106, no. 11, 2015, Art. no. 111908.

[32] L. Peng, C. Zhang, H. Wu, P. Yi, X. Lai, and J. Ni, "Continuous fabrication of multiscale compound eyes arrays with antireflection and hydrophobic properties," *IEEE Trans. Nanotechnol.*, vol. 15, no. 6, pp. 971–976, Nov. 2016.

[33] D. S. Ghosh, T. L. Chen, and V. Pruneri, "High figure-of-merit ultrathin metal transparent electrodes incorporating a conductive grid," *Appl. Phys. Lett.*, vol. 96, no. 4, 2010, Art. no. 041109.
[34] X. Heng and C. Luo, "Flexible PDMS microtubes for examining local hydrophobicity," *Microsyst. Technol.*, vol. 21, no. 2, pp. 477–485, 2015.
[35] Z. Yu *et al.*, "Highly flexible silver nanowire electrodes for shape-memory polymer light-emitting diodes," *Adv. Mater.*, vol. 23, no. 5, pp. 664–668, 2011.
[36] A. Khan, K. Rahman, D. S. Kim, and K. H. Choi, "Direct printing of copper conductive micro-tracks by multi-nozzle electrohydrodynamic inkjet printing process," *J. Mater. Process. Technol.*, vol. 212, no. 3, pp. 700–706, 2012.
[37] M. Vosgueritchian, D. J. Lipomi, and Z. Bao, "Highly conductive and transparent PEDOT: PSS films with a fluorosurfactant for stretchable and flexible transparent electrodes," *Adv. Funct. Mater.*, vol. 22, no. 2, pp. 421–428, 2012.
[38] J. Wu *et al.*, "Organic light-emitting diodes on solution-processed graphene transparent electrodes," *ACS Nano*, vol. 4, no. 1, pp. 43–48, 2010.
[39] A. R. Rathmell, S. M. Bergin, Y.-L. Hua, Z.-Y. Li, and B. J. Wiley, "The growth mechanism of copper nanowires and their properties in flexible, transparent conducting films," *Adv. Mater.*, vol. 22, no. 32, pp. 3558–3563, 2010.
[40] Y.-M. Choi, E.-S. Lee, T.-M. Lee, and K.-Y. Kim, "Optimization of a reverse-offset printing process and its application to a metal mesh touch screen sensor," *Microelectron. Eng.*, vol. 134, pp. 1–6, 2015.

Authors' photographs and biographies not available at the time of publication.